Research Square

Preprints are preliminary reports that have not undergone peer review.
They should not be considered conclusive, used to inform clinical practice,
or referenced by the media as validated information.

A novel VRS5 isoform untangles pleiotropic effects on barley tillering and row-type

Wilma van Esse

wilma.vanesse@wur.nl

Wageningen University & Research https://orcid.org/0000-0001-5012-2346

Ton Winkelmolen

Wageningen University and Research https://orcid.org/0009-0001-1178-3501

Pierangela Colleoni

Wageningen University and Research https://orcid.org/0009-0003-8061-2567

Marijke Hartog

Wageningen University and Research

Parastoo Hoseinzadeh

KWS SAAT SE & Co. KGaA

Ralf-Christian Schmidt

BASF Belgium Coordination Center CommV

Richard Immink

Wageningen University & Research https://orcid.org/0000-0002-0182-4138

Article

Keywords:

Posted Date: July 24th, 2026

DOI: https://doi.org/10.21203/rs.3.rs-10269004/v1

License: This work is licensed under a Creative Commons Attribution 4.0 International License.
Read Full License

Additional Declarations: There is **NO** Competing Interest.

A novel VRS5 isoform untangles pleiotropic effects on barley tillering and row-type

Ton Winkelmolen[1], Pierangela E. Colleoni[1], Marijke Hartog[1], Parastoo Hoseinzadeh[2], Ralf-Christian Schmidt[3], Richard G. H. Immink[1,4,5], and G. Wilma van Esse[1]*

[1]Laboratory of Molecular Biology, Wageningen University and Research, 6708 PB Wageningen, The Netherlands

[2]KWS SAAT SE & Co. KGaA, 37574 Einbeck, Germany

[3]BASF Belgium Coordination Center CommV, Technologiepark 101, 9052 Gent Zwijnaarde, Belgium

[4]Bioscience, Wageningen Plant Research, Wageningen University and Research, 6708 PB Wageningen, The Netherlands

[5]Current affiliation: Laboratory of Cell and Developmental Biology, Wageningen University and Research, 6708 PB Wageningen, The Netherlands

*Author for correspondence: wilma.vanesse@wur.nl

Abstract

The transcription factor *TEOSINTE BRANCHED1 (TB1)* and its orthologs were pivotal to cereal domestication. TB1 suppresses tillering but also influence inflorescence architecture and other yield-related traits, raising the question whether these functions can be molecularly separated. Here we show that the barley *TB1* ortholog *VULGARE ROW-TYPE SIX 5 (VRS5)*, which regulates both tiller bud outgrowth and lateral spikelet development, generates two transcript isoforms, *VRS5α* and *VRS5β*. Targeted mutagenesis of *VRS5α*, while retaining the downstream *VRS5β* transcript, increased tillering but maintained two-rowed spike architecture, genetically uncoupling vegetative branching from row-type regulation. Mechanistically, VRS5α and VRS5β showed promoter- and COMPOSITUM 1 (HvCOM1)-dependent differences in DNA binding: both isoforms bound the promoter of *VRS1*, a core regulator of row-type, in absence or presence of HvCOM1; in contrast, VRS5α, but not VRS5β, binds to the promoter of *HvGT1*, a regulator associated with tiller repression, in the presence of HvCOM1. These findings show that alternative transcript isoforms of VRS5 can be used to uncouple pleiotropic functions.

Introduction

Modification of plant architectural traits has been a central strategy in crop improvement since the earliest stages of domestication, when humans started to select enhanced performance and resilience in a particular growth habit[1]. A classic example is the suppression of spike brittleness to prevent natural dispersal of seeds, a trait that was targeted in major cereals such as rice, wheat and barley[2–4]. Shoot architecture has played a similarly central role, as underscored by the success of the green revolution with semidwarf rice (Oryza sativa) and wheat (Triticum aestivum) cultivars carrying reduced-height alleles such as *semi-dwarf1 (sd1)*, which conferred lodging resistance and improved harvest index under high-input conditions[5,6]. Similarly, the domestication of maize (*Zea mays*) from its wild ancestor teosinte (*Z. mays ssp. parviglumis*) required discarding highly branched phenotypes in favor of a single dominant stem bearing a terminal tassel and paired lateral ears, a transformation largely orchestrated by the increased expression of the *TEOSINTE BRANCHED1* (*TB1*) gene[7]. The pursuit of maintaining or increasing crop productivity under more extreme and variable climate conditions, through optimization of plant architecture, stands as both a promising frontier and an enduring challenge[8]. Yield is a complex trait, governed by not a single attribute but by an interplay between interdependent components such as grain number and size, branching patterns, and inflorescence architecture. Changing one of these yield components often influences others, making it hard to optimize yield through changing a single trait. The correlations that underlie tradeoffs have been well described in cereals. For example, enhancing grain number often reduces grain size due to limitations in resource allocation[9,10]. While resource distribution plays a role in yield-related trade-offs, it is not the sole factor; genetic regulation, hormonal signaling, and developmental timing also contribute to these complex interdependencies. Recent studies suggest that overlapping developmental windows for grain number and grain size determination also contribute to this trade-off[11,12]. Moreover, genetic analyses have revealed that many loci influencing grain number and grain weight co-localize and exert inverse effects, indicating a strong genetic basis for this trade-off[12,13]. Similarly, genes that influence both shoot and inflorescence architecture often act across multiple developmental axes, which makes the genetic decoupling of these traits inherently difficult[14]. *TB1* was targeted during the domestication of several cereal crops for its role in tiller development[15–18]. Beyond tillering, *TB1* also affects inflorescence determinacy, plant height, and root architecture, underscoring its pleiotropic impact on plant form[19–22]. Similar multifunctionality has been observed across cereals: in barley, its ortholog *VRS5/INT-C* regulates tillering and spikelet fertility[14,17]; in wheat, elevated *TB1* dosage alters growth rate, spikelet number, and shoot morphology[19,20]. Despite these insights, whether TB1-dependent vegetative and reproductive traits can be genetically decoupled has remained unclear, highlighting a regulatory constraint shared across cereal species.

We performed a phylogenetic analysis of TB1 orthologs across monocots and identified a conserved internal methionine within *Poaceae* TB1 proteins, suggesting that these proteins may have the capacity to form a shorter isoform. Using barley, we show that the TB1 ortholog *VRS5* produces two transcript isoforms through alternative transcription start site usage: a long *VRS5α* transcript and a shorter *VRS5β* transcript predicted to encode an N-terminally truncated protein. Through targeted mutagenesis, we generated lines in which the long *VRS5α* isoform is disrupted while the downstream *VRS5β* region is retained. These lines uncouple canonical *vrs5* phenotypes, increasing tillering while maintaining two-rowed spike architecture. We further show that the predicted VRS5 isoforms differ in their ability to bind target promoters in combination with HvCOM1, providing a mechanistic basis for isoform-specific regulation.

Together, our results reveal alternative transcription start site usage as a mechanism that can partition pleiotropic functions of a cereal domestication regulator.

Results

Alternative transcription start site usage generates two VRS5 transcript isoforms

TB1 and BRANCHED1 (BRC1) are members of the CYC/TB1 subgroup of class II TCP transcription factors in plants[23]. Phylogenetic analysis across monocots and dicots places TB1 and BRC1 in distinct clades consistent with divergence following the monocot-dicot split (**Figure S1, Table S1, Table S2**). Within the monocots, the TB1 clade contains ZmTB1, OsTB1, VRS5, and the *Triticeae*-specific TB1-like. The grass-specific sister clade includes BRANCHED ANGLE DEFECTIVE 1 (ZmBAD1), and barley COMPOSITUM 1 (HvCOM1; also referred to as HvTB2)[24,25]. Alignment of TB1 orthologs revealed, aside from the classical TCP, R and SP domains, a highly conserved internal methionine residue in VRS5, ZmTB1 and OsTB1 (**Figure 1A, Figure S2**). This residue is absent from the TB1-like and BAD1/COM1 lineages, indicating that it is restricted to a core grass TB1 subclade. The positional conservation of this methionine suggested that grass TB1 proteins may produce a shorter isoform. Such an isoform could arise either through alternative translation initiation (aTIS) or through alternative transcription start site (aTSS) usage. To test the latter possibility, we reanalyzed long-read PacBio Iso-Seq datasets from pooled barley RNA[26] and maize RNA[27], which capture full-length transcripts and enable detection of transcript 5′ ends. In barley, two distinct VRS5 transcripts were detected (**Figure 1B**), consistent with aTSS usage. The shorter transcript (VRS5β) initiates downstream of the annotated translation start codon of the full-length VRS5α isoform. The VRS5β transcript is predicted to encode an N-terminally truncated VRS5 protein starting at the conserved internal methionine, lacking the SP domain but retaining the TCP and R domains. VRS5α and VRS5β are predicted to encode proteins of 357 and 274 amino acids, respectively. Long-read data from maize similarly supported the presence of alternative TB1 transcripts, albeit at lower coverage (**Figure S3**). To further characterize isoform expression in barley, we performed qPCR using isoform-specific primer sets. Three developmental stages at which *VRS5* is expressed were sampled: double ridge (DR), lemma and stamen primordia (LP/SP), and awn primordia (AP). Significant differences between total VRS5 transcript levels and VRS5α-specific transcript levels were observed at the DR and AP stages. At DR and AP, VRS5α accounted for approximately half of the total VRS5 expression, indicating that the shorter VRS5β transcript contributes substantially to VRS5 transcript abundance (**Figure 1C**). Together, our results show that VRS5 produces two transcript isoforms through aTSS usage.

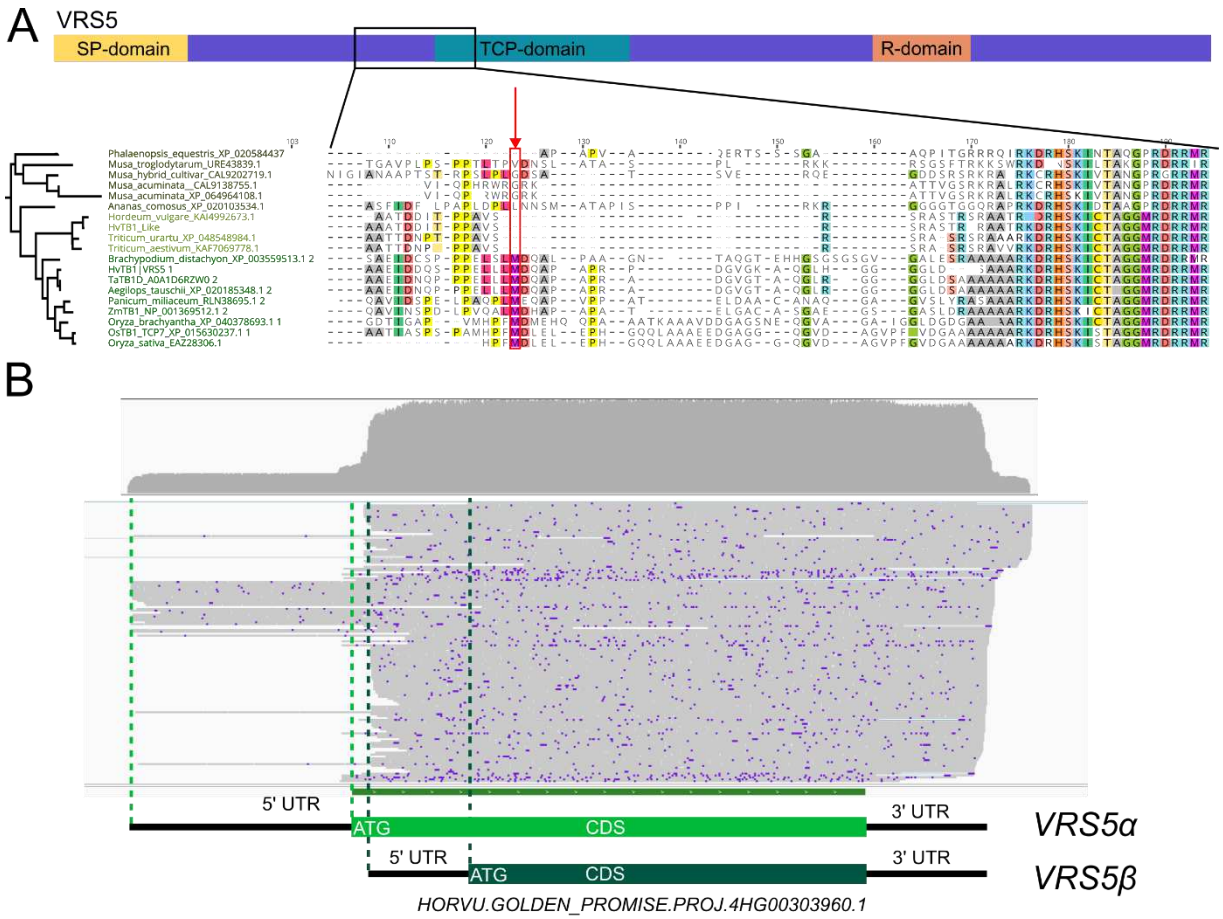


Figure 1. Conserved domains in TB1, and closely related orthologs. A) Protein alignment of TB1 and closely related TCPs from various species showing the conserved methionine specifically in the TB1 sub-clade. B) Alignment of long-read RNA sequencing reads of pooled barley RNA of cv. Barke[26] mapped to the *VRS5* locus in Golden Promise[28]. The dashed lines indicate the transcription start sites (TSSs) and start codons (ATGs) of *VRS5α* and *VRS5β*. The schematic below shows the two VRS5 isoforms and their corresponding coding sequences (CDS). C) qPCR of *VRS5* isoforms in cv. Golden Promise relative to *HvActin* at different developmental stages: double ridge (DR), Lemma and stamen primordia (LP/SP), and awn primordia (AP). Primers for *VRS5α* are designed on the 5'UTR of *VRS5α* to only amplify the long *VRS5α* transcript. Primers that amplify both *VRS5* transcripts are designed on the CDS that is shared between both transcripts. Statistical differences between *VRS5α* and total *VRS5* transcripts is calculated using a paired t-test with asterisks indicating significance (*: p<0.05, **: p<0.01). n = 3 biological replicates.

Control of tillering and row-type through different VRS5 isoforms

The shorter transcript, *VRS5β*, starts downstream of the annotated translation start codon present in the long *VRS5α* transcript. Consequently, translation from the canonical VRS5 start codon cannot occur in this transcript (**Figure 1B**). We hypothesize that the conserved methionine in VRS5 (**Figure 1A**) serves as a translation start site in the shorter transcript, resulting in the formation of the predicted VRS5β protein (**Figure 1B**). Predictive modeling using AlphaFold suggests that both VRS5α and VRS5β would give rise to DNA-binding proteins, with the main difference being the absence of the SP domain in the VRS5β isoform, while the DNA-binding TCP domain remains unaltered (**Figure S4**). To understand the function of the two VRS5 isoforms in barley, we performed gene editing to generate lines in which the long VRS5α isoform is disrupted while the downstream VRS5β coding region remains intact. This resulted in two independent lines, *vrs5α-1* and *vrs5α-2*, each carrying deletions within the VRS5α coding sequence that introduce a frameshift mutation, while the genomic region corresponding to the VRS5β coding sequence remains unaltered (**Figure 2A, Figure S5A**).

To confirm that these mutations specifically disrupt the VRS5α transcript while retaining transcription of the VRS5β region, we analysed RNA-seq datasets from double ridge (DR) and lemma and stamen primordia (LP/SP) tissues. In *vrs5α-1*, coverage across the 5′ region corresponding to VRS5α was strongly reduced compared with GP, whereas transcription across the downstream region shared with VRS5β was retained, although overall VRS5 expression was reduced relative to WT (**Figure S5C**). For phenotypic comparison in an isogenic background, we also included a full knockout of both isoforms, *vrs5,* which has an 857bp deletion (**Figure 2A, Figure S5A**). The *vrs5* mutant showed a significantly increased tiller number compared to WT and an intermediate row-type phenotype (**Figure 2B,C,D**), corroborating previous reports[14,17,29].

Differences in plant height and flag leaf emergence were also observed between *vrs5* and WT (**Figure S6A,B,C**), as reported previously [29]. Intriguingly, *vrs5α-1* and *vrs5α-2*, which express only the short *VRS5β* transcript, showed a significantly increased tiller number compared to WT (**Figure 2B**), while maintaining a two-rowed spike similar to WT (**Figure 2C,D**). This indicates that expression of VRS5β alone is sufficient to maintain the two-rowed spike phenotype, but insufficient to repress tiller development. Moreover, although *vrs5α* mutant spikes are two-rowed, the spikes are shorter, and the central spikelets are smaller compared to WT, similar to *vrs5* (**Figure S7, Figure S8**). Expression of the downstream VRS5β transcript in the absence of functional VRS5α thus uncouples the tillering and row-type phenotypes associated with *vrs5*. In addition, VRS5β expression separates row-type determination from other spike architectural traits, including spike length and central spikelet size. Taken together, our results show that VRS5 isoforms contribute differently to barley architecture: the long VRS5α isoform is required to repress tiller development, whereas the short VRS5β isoform is sufficient to maintain lateral spikelet suppression and two-rowed spike architecture.

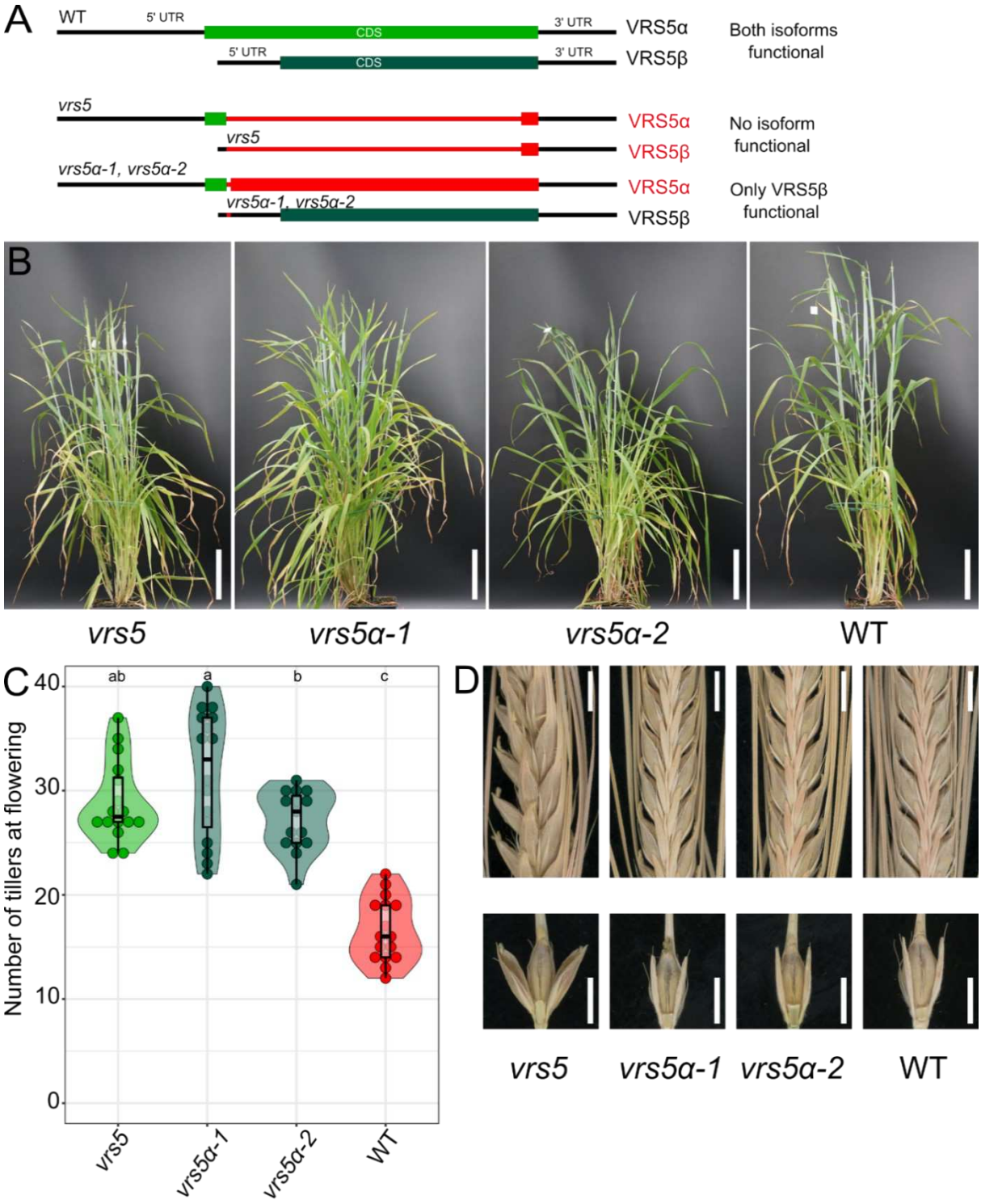


Figure 2. CRISPR mutagenesis of VRS5 uncouples pleiotropic effects on tillering and row-type. A) schematic protein overview of both VRS5α and VRS5β and the created mutants. B) Plant pictures of *vrs5α* lines compared to the full knockout *vrs5* and WT (cv. Golden Promise). Pictures were taken at flowering, defined as heading date. The white bars represent a length of 10 cm. C) Number of tillers at flowering of *vrs5α* and *vrs5* lines in comparison to WT (cv. Golden Promise). Significant differences are calculated using a one-way ANOVA followed by Tukey's HSD. Different letters indicate significant differences between the lines ($p<0.05$). $n \geq 12$ biological replicates. D) Spike phenotype of *vrs5α* lines compared to the full knockout *vrs5* and WT (cv. Golden Promise). Lower images show triple spikelets, showing developed lateral spikelets for *vrs5* only. The white bars represent a length of 0.5 cm.

VRS5 regulates row-type through interaction with HvCOM1

Phenotypically, the *vrs5* mutants showed a six-rowed intermediate spike architecture, while *vrs5α-1* and *vrs5α-2* have a two-rowed spike architecture (**Figure 2D**). We therefore hypothesized that both isoforms are still capable of binding to the promoter of *VULGARE ROW-TYPE SIX1 (VRS1; HORVU.MOREX.r3.2HG0184740)* to regulate its expression. This gene is directly downstream of VRS5 in the regulation of lateral spikelet development[30]. To test this hypothesis, we performed an Electrophoretic Mobility Shift Assay (EMSA) on the *VRS1* promoter fragment containing the VRS5 binding site. These experiments confirmed that both VRS5α and VRS5β can bind to the VRS5 binding site present in the promoter of *VRS1* (**Figure 3A**). Previously, it was shown that another class II TCP transcription factor, HvCOM1 (also referred to as HvTB2) can interact with VRS5[24]. Moreover, our DNA Affinity Purification Sequencing (DAP-Seq) of VRS5 and HvCOM1 showed that both VRS5 and HvCOM1 bind to the same region within the VRS1 promoter (**Figure 3B**). We therefore hypothesized that VRS5 and HvCOM1 may together bind in a protein complex to the *VRS1* promoter. To test this hypothesis, we performed an EMSA to evaluate the interaction of the VRS5α/HvCOM1 and VRS5β/HvCOM1 protein complexes with the *VRS1* promoter. These experiments confirmed that both VRS5 isoforms, HvCOM1, as well as the VRS5α/HvCOM1 and VRS5β/HvCOM1 complexes can bind to the *VRS1* promoter fragment (**Figure 3C, Figure S9A,C**). This also suggests that VRS5 and HvCOM1 may act at least partially together in the regulation of row-type through *VRS1*. To test this genetically, we generated *vrs5com1* double mutants. The *vrs5com1* double mutants have fully fertile awned lateral spikelets that develop into grains (**Figure 3D**). These lateral spikelets of *vrs5com1* are wider and heavier compared to *vrs5* lateral spikelets (**Figure 3E-3G**), showing an additive effect on lateral spikelet development compared to the *vrs5* single mutant (**Figure 3D**). Consistent with a role for VRS5 and HvCOM1 in VRS1 regulation, *VRS1* expression was significantly downregulated in the *vrs5* and *vrs5com1* mutants at the lemma and stamen primordium (LP/SP) stage, while VRS1 expression in vrs5α was not significantly reduced (**Figure 3H**). Moreover, *vrs5αcom1*, which can still express *VRS5β*, showed no six-rowed spike architecture, but a spike resembling *com1,* with indeterminate spikelets at the basal part of the spike, and further two-rowed (**Figure 3D**)[24,25,31]. In addition, RNA-seq of developing inflorescences of *vrs5, com1,* and *vrs5com1* compared to their respective WT at double ridge (DR) and lemma and stamen primordia (LP/SP) revealed overlapping sets of differentially expressed genes (DEGs) and enriched GO-terms within these DEGs (**Figure S10**), consistent with partially shared roles for VRS5 and HvCOM1 in gene regulation.

Together, our data suggest that VRS5 and HvCOM1 have additive genetic effects on lateral spikelet development and partially converge on VRS1 regulation. In addition, the absence of a row-type phenotype in *vrs5α* and *vrs5αcom1* mutants indicates that VRS5β is sufficient to maintain VRS1 expression and two-rowed spike architecture.

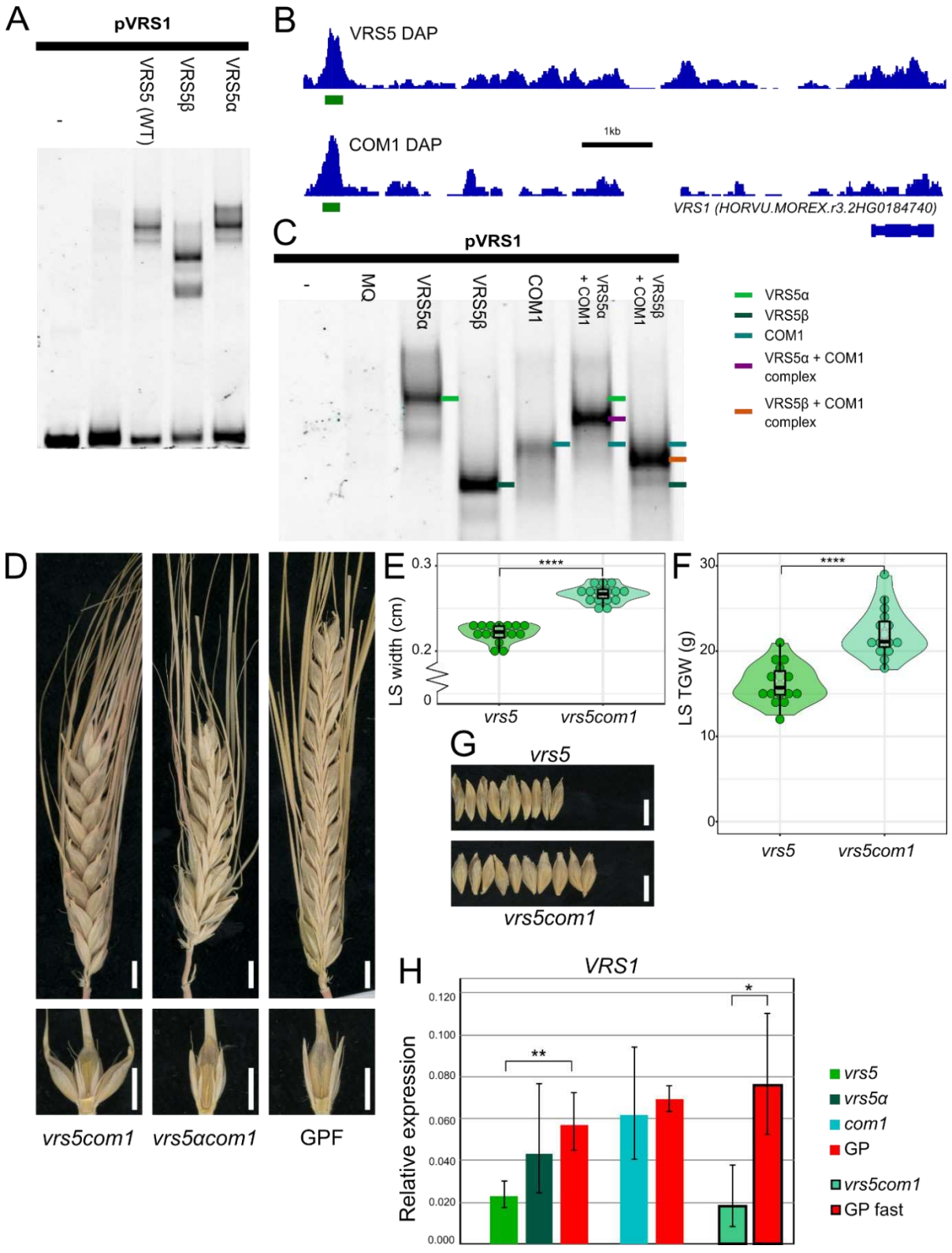


Figure 3. HvCOM1 has an additive effect to VRS5 on the regulation of row type. A) EMSA of VRS5 isoforms binding to a labeled DNA probe containing the VRS5 binding site in the promoter of *VRS1*. B) DAP-Seq trace file of the *VRS1* promoter showing DAP-Seq peaks for both VRS5 and HvCOM1; C) EMSA of VRS5 isoforms and HvCOM1 binding to a labeled DNA probe containing the TCP binding site in the DAP peak of VRS5 and HvCOM1 in the promoter of *VRS1* (pVRS1). The colored bars represent the expected heights of the protein complexes. D) Spike images of *vrs5com1, vrs5αcom1*, and WT (cv. Golden Promise Fast,GPF). Lower images show triple spikelets, with developed lateral spikelets observed in *vrs5com1* only.

White scale bars represent 0.5 cm. Plots showing E) Average lateral spikelet (LS) width and F) lateral spikelet (LS) thousand grain weight (TGW) of *vrs5* and *vrs5com1*. Significant difference was calculated using a One-way ANOVA, with asterisks indicating significance (****: p<0.0001). n ≥ 15 biological replicates. G) Representation of lateral spikelet width showing 10 lateral spikelets of *vrs5* and *vrs5com1.* White bars indicate a length of 0.5 cm. H) qPCR showing relative expression of *VRS1* compared to *HvActin* in developing inflorescences at lemma and stamen primordium (LP/SP) stage in *vrs5, vrs5α, com1,* cv. Golden Promise (GP), *vrs5com1* and cv. Golden promise fast (GPF). Error bars indicate standard deviation. n = 3 biological replicates. Asterisks indicate statistical significance calculated using a Student's t-test between the mutants and their corresponding WT (* : p<0.05, ** : p<0.01).

VRS5 isoforms show altered binding to the *HvGT1* promoter

In the regulation of row-type, both VRS5 isoforms bind to the VRS1 promoter together with HvCOM1. This is in line with the two-rowed spike architecture of the *vrs5α-1* and *vrs5α-2* lines, in which only the short VRS5β isoform can be formed. However, the presence of a tillering phenotype in these lines **(Figure 2C)** suggests that the long *VRS5α* is essential for the regulation of tiller bud outgrowth. Previously, it was shown that in maize and Arabidopsis, TCP transcriptional regulators regulate bud outgrowth through homeobox transcription factors closely related to VRS1; GRASSY TILLERS (ZmGT1) in maize, directly downstream of ZmTB1 [32,33], and HOMEOBOX PROTEINS (HB21, HB40, and HB53) in *Arabidopsis,* directly downstream of BRANCHED1 (BRC1)[34]. To measure expression of *HvGT1* in barley *vrs5* and *com1* lines, we performed qPCR on crown tissue of the mutant lines at the double ridge stage. We show that *HvGT1* expression was significantly downregulated in *vrs5* and *com1,* as well as in *vrs5com1* (**Figure 4A**). We therefore postulated that the role of *GT1* in axillary bud outgrowth and its upstream regulation may be conserved across species. In barley, *HvGRASSY TILLERS* (*HORVU.MOREX.r3.4HG0399240*) has been described in relation to tip degeneration, and mutants in this gene produced more rachis nodes[35]. We generated two independent mutants of *HvGT1*, *gt1-1* and *gt1-2*. These lines indeed showed an increased number of rachis nodes, corroborating previous reports (**Figure S11**)[35]. As postulated, both *gt1-1* and *gt1-2* showed an increased number of tillers compared to WT (**Figure 4B**), similar to *vrs5* (**Figure 4B**), indicating its importance in the regulation of tiller bud outgrowth. Although *HvGT1* is downregulated in *vrs5*, no direct binding of VRS5 to the *HvGT1* locus was observed in our DAP-Seq experiment (**Figure 4C**). In contrast, the DAP-Seq of HvCOM1 showed a peak ~ 1kb upstream of *HvGT1* (**Figure 4C**). To confirm binding of HvCOM1 to this region, an EMSA was performed using the TCP binding site in the COM1 binding peak as a probe. HvCOM1 was able to bind to the *HvGT1* promoter fragment, while neither of the VRS5 isoforms was, corroborating both DAP-Seq experiments (**Figure 4D**). We also tested the binding of the VRS5/HvCOM1 protein complexes. VRS5*α* was only able to bind to the *HvGT1* promoter in the presence of HvCOM1. This suggests that VRS5 requires HvCOM1 to bind to the *HvGT1* promoter (**Figure 4D, Figure S9B,D**). Intriguingly, VRS5β was unable to bind to the *HvGT1* promoter, even in the presence of HvCOM1 (**Figure 4D, Figure S9B,D**). This indicates that the long VRS5α isoform is required for binding of the VRS5/COM1 complex to the *HvGT1* promoter, suggesting that VRS5α is essential to regulate tillering, at least in part, via *HvGT1*. This corresponds to our observation that both *vrs5α* and *com1* showed a significant increase in tillering (**Figure 2B,C, Figure 4B**). In line with this, also the *vrs5com1* and *vrs5αcom1* showed an increased number of tillers at flowering compared to WT (**Figure 4E**). Taken together, VRS5 binding to the HvGT1 promoter depends on the isoform and the presence of

HvCOM1. This provides a mechanistic basis for isoform-specific control of HvGT1 expression and its associated role in regulating tiller development.

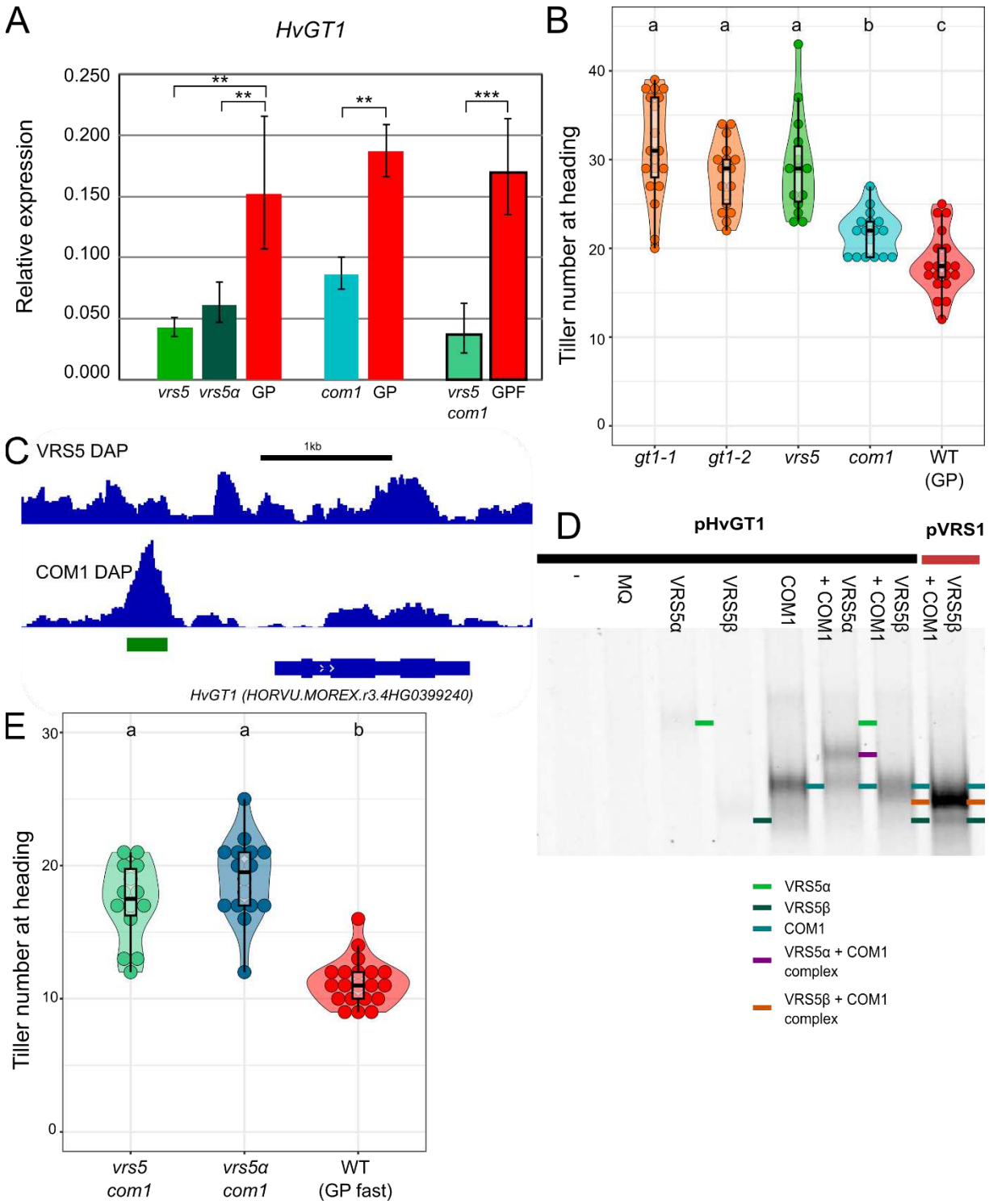


Figure 4: The long VRS5α isoform is required for repression of tiller outgrowth. A) qPCR showing relative expression of *HvGT1* compared to *Actin* in crown tissue at the double ridge stage in *vrs5, vrs5α, com1,* cv. Golden Promise (GP), *vrs5com1,* and cv. Golden promise fast (GPF). *vrs5, vrs5α,* and GP are grown together, whereas *com1* and another GP are grown at a different time. Therefore, both corresponding GP controls are shown. Error bars indicate standard deviation. n = 3 biological replicates. Asterisks indicate statistical significance

calculated using a Student's t-test between the mutants and their corresponding WT controls (** : p<0.01, *** : p<0.001). B) Tiller number of *vrs5, com1, gt1-1, gt1-2*, and WT (cv. GP) at flowering. Different letters indicate significant differences ($p < 0.05$) between the lines, calculated using Kruskal-Wallis test followed by Dunn's to adjust for multiple testing. $n \geq 14$ biological replicates. C) DAP-Seq trace file of *HvGT1* promoter. The bar below the trace file shows significant enrichment compared to control for HvCOM1, but not VRS5. D) EMSA of VRS5 isoforms and HvCOM1 binding to a labeled DNA probe containing the TCP binding site in the DAP peak of HvCOM1 in the promoter of *HvGT1* (*pHvGT1*). The colored bars represent the expected heights of the protein complexes. To show that the VRS5α/COM1 complex was formed, binding of that complex to an infrared-labeled DNA probe containing the TCP binding site in the DAP peak of VRS5 and HvCOM1 in the promoter of *VRS1* (*pVRS1*) was shown in the last lane. E) Tiller number of *vrs5com1, vrs5αcom1*, and WT (cv. GPF) at flowering. Significance was calculated using One-way ANOVA followed by Tukey's HSD. Different letters indicate significant differences between the lines ($p < 0.05$). $n \geq 14$ biological replicates.

Discussion

Alternative transcription start site (aTSS) usage represents a powerful mechanism to expand the functional output of a single gene by generating transcript and protein isoforms with distinct regulatory potential. Transcriptome-wide studies have revealed extensive transcription start site variation and promoter plasticity in plants, including cereals, and alternative transcript variants generated through aTSS usage and alternative splicing are widespread[36–43]. However, despite accumulating evidence for transcript diversity, the phenotypic consequences of selectively disrupting individual transcript isoforms remain largely unexplored. Here, we show that the barley TB1 ortholog VRS5 produces two transcript isoforms, *VRS5α* and *VRS5β*, through aTSS usage. Targeted mutagenesis of the long *VRS5α* isoform, while retaining the downstream *VRS5β* transcript, uncoupled canonical *vrs5* phenotypes: *vrs5α* mutants showed increased tillering but retained two-rowed spike architecture. These findings reveal that pleiotropic functions of VRS5 are separable at the transcript isoform level.

The phenotypes of the *vrs5α* mutants further indicate that *VRS5*-dependent traits are modular, but not simply divided into two independent outputs. While row-type was uncoupled from tillering, *vrs5α* spikes were still shorter and had smaller central spikelets compared to WT, similar to full *vrs5* mutants. Thus, *VRS5β* is sufficient to maintain two-rowed spike architecture, but not all *VRS5*-dependent spike and grain traits. Effects of VRS5 on grain size have often been attributed to source-sink relationships associated with the development of lateral spikelets acting as additional sinks[14,44,45]. Because *vrs5α* mutants remain two-rowed but still show a reduced central spikelet size when compared to the wild type, these effects cannot be explained solely by the development of fertile lateral spikelets as additional sinks. They may instead reflect a direct role of *VRS5* in spike and grain development, indirect effects of altered whole-plant source–sink balance due to increased tillering, or both. Together, alternative *VRS5* isoform usage separates row-type from tillering, while revealing additional VRS5-dependent architectural outputs that are not simply explained by row-type changes.

Recently, we showed that VRS5 binds directly to the *VRS1* promoter to regulate its expression[30]. *VRS1* is a well-known barley row-type regulator that acts downstream in the VRS network to suppress lateral floret development[46]. Mutations in *vrs1* result in a complete six-rowed spike architecture, while a full *vrs5* knockout has an intermediate six-rowed phenotype, suggesting that VRS5 is not the only regulator of VRS1 expression. Here, we show that HvCOM1, a class II TCP transcription factor previously shown to interact with VRS5[24,25,31] also binds the VRS1 promoter and genetically contributes to lateral spikelet suppression. The enhanced lateral spikelet development of *vrs5com1* compared with *vrs5* indicates additive genetic effects on row-type regulation. At the same time, *vrs5α* and *vrs5αcom1* mutants did not show six-rowed spike architecture, supporting the conclusion that VRS5β retains sufficient activity to maintain *VRS1* expression and two-rowed spike architecture. Thus, VRS5 and HvCOM1 partially converge on the VRS1-dependent row-type module, while HvCOM1 also retains distinct roles in spikelet determinacy.

The behavior of VRS5 isoforms differed between the *VRS1* and *HvGT1* regulatory contexts. At the *VRS1* promoter, both VRS5α and VRS5β were able to bind, either alone or in combination with HvCOM1. By contrast, at the *HvGT1* promoter, VRS5α binding was detected only in the presence of HvCOM1, whereas VRS5β did not bind, even with HvCOM1. GT1-related HD-ZIP transcription factors act downstream of TCP regulators in bud outgrowth pathways in maize and Arabidopsis, and HvGT1 has also been linked to tillering in barley[32,34,35]. Together, our findings suggest that VRS5 isoforms do not simply differ in activity, but in their ability to interact with distinct promoter regions and protein complexes. The distinct

protein-DNA and protein-protein interactions of the isoforms provide a mechanistic basis for the phenotypic uncoupling observed in the *vrs5α* mutants. The weaker tillering phenotype of *com1* compared with *vrs5* or *gt1* further suggests that HvCOM1 is not a simple obligate cofactor for all VRS5-dependent tiller functions, but may facilitate VRS5α activity at specific regulatory elements. Defining how these isoform-specific interactions vary across developmental stages and regulatory contexts represents an important next step toward understanding how these isoforms orchestrate plant development and adaptive plasticity in response to internal and external cues. Although our study focuses on the interaction between VRS5 and HvCOM1, previous work showed that VRS5 can interact with additional class II TCP transcription factors. TB1-dependent developmental regulation may therefore involve multiple TCP-containing complexes that act in distinct developmental contexts.

Our findings show that aTSS usage can expose hidden modularity within a pleiotropic cereal domestication regulator. Using targeted mutagenesis of VRS5α, while retaining VRS5β, we genetically separated tillering from row-type regulation, revealing that specific vegetative and reproductive outputs of *VRS5* can be partitioned at the isoform level. This suggests that pleiotropy at key developmental regulators is not always fixed at the gene level, but can reside in separable isoform-dependent regulatory modules. More broadly, even deeply conserved pleiotropic genes such as *TB1* in *Poaceae* may retain functional plasticity, offering a mechanism through which pleiotropy at the gene level can be partially bypassed. Future work should determine how aTSS choice is controlled across developmental stages, genetic backgrounds and environmental conditions, and whether similar isoform-level partitioning operates at other pleiotropic loci. Such knowledge could provide new entry points for precision breeding, enabling specific architectural traits to be modified without complete loss of gene function.

Materials & Methods

CRISPR mediated mutagenesis

CRISPR-Cas9 mediated mutagenesis of *VRS5,* and *HvGT1* was performed using the previously described in-house CRISPR vector system[30]. For each target, three guides were designed (**Table S4**) and cloned into an optimized Cas9 scaffold under control of the TaU6 promoter[47,48], available at Addgene: ID:231030 - 231033. The final level 2 vector used for *in-planta* transformation contained the intron-optimized hygromycin resistance cassette (pICSL11059), the Cas9 expression cassette (pICSL11056), and three guide RNAs specific for the targeted gene. The construct was cloned in the hypervirulent *Agrobacterium tumefaciens* strain *AGL1 pSOUP,* and used for *Agrobacterium*-mediated transformation of barley cv. Golden Promise immature embryos[49]. T_0 plants were genotyped for CRISPR mutations using the Phire Plant Direct PCR Kit (Thermo Fisher Scientific) using primers described in **Table S4**. Amplified fragments were sequenced directly. For the generation of double mutants, the codon-optimized Cas9 containing 13 introns and two nuclear localization signals (pAGM47523) was used [50] in combination with four guide RNAs; two targeting *VRS5*, and two targeting *HvCOM1* (**Table S4**).

Phenotyping

For the phenotyping of the *vrs5* mutants, seeds of *vrs5, vrs5α-1, vrs5α-2* **(Figure S5A)***,* and Golden Promise (WT) were sown in square 1.3L pots containing soil. To phenotype the *hvgt1* mutants, seeds of *gt1-1, gt1-2, vrs5, com1-1* **(Figure S5A, S10A)***,* and Golden Promise (WT) were sown in square 1.3L pots containing soil. For phenotyping of the *vrs5com1* mutants, seeds of two primary transformants and Golden Promise Fast (WT) were sown in 84-well trays containing soil. To equalize germination, the pots or trays were kept at 4°C in the dark for 5 days, before putting them in the greenhouse. Plants were grown in the greenhouse (16h light 21°C, 8h dark 18°C). The plants in the trays were genotyped for *VRS5, HvCOM1, and* Cas9 as described above. After genotyping, a selection of plants that are either *vrs5com1* or *vrs5αcom1* were repotted in square 1.3L pots containing soil. Also, WT plants were repotted in the same way. *Vrs5com1* and *vrs5αcom1* are a mix of plants that still contain the *Cas9* gene and plants that no longer contain the *Cas9* gene. For each round of phenotyping, tiller number per plant was recorded twice a week until flowering. After harvest, three spikes of each plant, including the main spike, were measured for spike length and number of rachis nodes. After that, the individual seeds per spike were scanned using an Epson V850 Pro scanner. Using ImageJ, the seed dimensions were analyzed and averaged per spike per plant. The total number of seeds of three spikes of a plant was weighed to impute thousand grain weight (TGW).

Electrophoretic mobility shift assay (EMSA)

EMSA was performed as described previously[30]. DNA probes of 50bp were designed from genomic DNA and synthesized (Biolegio). Probes were cloned into pGEM-T. The probes were labeled by PCR amplification using CY5.5-labeled primers. VRS5α CDS was synthesized by changing the ATG codon in VRS5 coding for a methionine into GCG, making it code for an alanine, making sure no VRS5β can be formed (**Table S4**). VRS5β CDS was cloned into pDONR201 using primers amplifying from the start codon of VRS5β to the stop codon (**Table S4**). COM1 CDS was cloned into pDONR201 using primers described (**Table S4**). All CDSs were amplified from genomic DNA from cv. Bowman. CDSs in pDONR201 were cloned into

an expression vector under the SP6 promoter[51]. VRS5, VRS5α, VRS5β, and COM1 proteins were prepared using TNT SP6 Wheat germ protein expression system (Promega). Combination of proteins were prepared by adding identical amount of each representative plasmid to the expression system. The EMSA binding reaction was performed for 45 minutes on ice using a binding reaction mixture (1.2 mM EDTA (pH 8.0), 0.25 mg/ml BSA, 7.2 mM HEPES (pH 7.3), 0.7 mM DTT, 60 µg/ml salmon sperm DNA, 1.3 mM spermidine, 2.5% CHAPS, 8% glycerol, 6.6 nmol/ml single-labelled dsDNA, and 2 µl of in vitro-synthesized proteins. The mixture was loaded on a 5% polyacrylamide gel and run in 1x TBE buffer for 180 minutes at 75V. The gels were scanned using a LiCor Odyssey Imaging system at 700nm. To visualize the free probes, the gels were also scanned after running for 90 minutes, after which the running of the gels was continued.

Phylogenetic analysis of TB1 clade

Protein sequences of *TEOSINTE BRANCHED1* (TB1) from maize (*Zea mays*), wheat (*Triticum aestivum*), and barley (*Hordeum vulgare*), as well as COMPOSITUM1 (COM1) from barley and BRANCH ANGLE DEFECTIVE1 (BAD1) from maize, were used as input for the blast search in NCBI against 48 plant species spanning monocots. Gene ID of the input sequences, as well as the target plant species, can be found in **Table S1** and **Table S2**. As input for the blastp we used VRS5(HvTB1), ZmTB1, TaTB1-D, AtBRC1, and SlBRC1. Using these sequences against the NCBI ClusteredNR database (clustered at 90% identity) enables fast and representative similarity searches while minimizing redundancy. The blast searches were performed using standard settings which are: Expected threshold, word size 5, matrix BLOSUM65, Gap Cost, Existence 11, extension 1, and conditional compositional score matrix adjustments. All blast hits were filtered to match records with: percent identity between 60 and 95%, expect value 1e-6; query coverage between 15 and 100. The barley gene TB1-like was added manually, as this gene is not present in the Morex V3 genome. Subsequently, all partial sequences and duplicates were removed, retaining in total 105 proteins, from both monocots and dicots, which were aligned using MUSCLE[52]. A maximum likelihood phylogenetic tree was constructed using RAxML[53], as described previously[24]. As outgroup, the blastp hit from *Amborella trichopoda* (ERN05207) was used. An Auto MRE model was used to assess convergence during bootstrapping, which was met after 400 bootstraps.

Long-read RNA-sequencing alignment

Previously published long-read RNA-sequencing data were used that contain RNA transcripts of a pool of barley tissues[26]. This dataset was realigned against the cv. Golden Promise reference genome from the barley pangenome[28]. Previously published long-read RNA-sequencing of maize containing RNA transcripts of the maize tassel and ears was used as well[27]. The reads were realigned against the NAM 5.0 B73 maize reference genome[54]. Raw reads were aligned using Minimap2[55]. For visualization of transcripts, IGV was used[56].

DAP-sequencing COM1

The COM1 CDS from cv. Bowman was cloned into the pSPUTK vector, where a 3xFLAG tag (pICSL50007) was fused C-terminally. As a negative control, 3xFLAG fused to GFP was used. For both COM1 and the negative control, three replicates were performed and sequenced. DAP-sequencing of COM1 was performed and the raw data were analyzed as described before for VRS5[30]. In the present study, analyses were focused on COM1 binding at the *VRS1*

and *HvGT1* promoter regions (**Table S3**), which were selected as candidate regulatory targets. Raw sequencing reads have been deposited in GEO under accession number GSE337394.

RNA isolation and quantitative PCR

Seeds of *vrs5, vrs5α-1, com1,* and WT (cv. Golden Promise), and *vrs5com1* and WT (cv. Golden Promise fast) were sown in soil in 84-well trays. The trays were kept at 4°C in the dark for three days to enhance equal germination. After that, the plants were transferred to a growth chamber under long day conditions (16h light/8h dark) at 20°C. To score the developmental stages, three plants of each genotype were dissected under a stereomicroscope using the Waddington scale[57]. Developing inflorescences were sampled at different stages: double ridge (DR), lemma and stamen primordia (LP/SP), and awn primordia (AP). Samples were immediately frozen in liquid nitrogen and stored at -80°C until RNA isolation. *vrs5, vrs5α*, and their corresponding GP control were grown together in one experiment, while *com1* and its GP control were grown separately in a different experiment. Therefore, both GP controls are shown, and statistical comparisons were made relative to the GP control used in each respective experiment. For each developmental stage and each genotype, three biological replicates were taken, consisting of ~10 developing inflorescences. RNA extraction and quantitative PCR was performed as described[30]. The primers used for quantitative PCR are described in **Table S4**. Extracted RNA samples that were used for RNA-seq were sent to Novogene Europe (Cambridge Science Park, United Kingdom), where mRNA was purified from total RNA. Samples were sequenced using the Illumina platform with a sequencing depth of 20 million reads per sample using 150 bp paired-end reads.

RNA-seq analysis and GO-term enrichment

Raw paired RNA-seq reads were trimmed using Trimmomatic v0.39[58] using parameters: ILLUMINACLIP:adapters.fa:2:30:10 LEADING:3 TRAILING:3 SLIDINGWINDOW:4:15 MINLEN:36. The file adapters.fa contains nucleotide sequences of Illumina adapters used for library construction. Transcripts were quantified using the MorexV3 as reference[59], using salmon[60] (**Table S5**). Per developmental stage, the differentially expressed genes (DEGs) of *vrs5, com1*, and *vrs5com1* compared to their respective wild-type controls (Golden Promise for *vrs5* and *com1*, Golden Promise Fast for *vrs5com1*) were determined using DESeq2[61] (**Table S6**).

GO-terms were assigned to the coding sequences of the MorexV3 reference genome[59] using Pannzer2[62]. GO-term enrichment was done on differentially expressed genes (DEGs) of each comparison using the R package clusterProfiler. Raw sequencing reads have been deposited in GEO under accession numbers GSE337501 and GSE337502.

AlphaFold protein modeling

To get the 3D prediction of the TCP dimers, we used AlphaFold3[63], accessed on: 03 June 2025. To include the crystallographic structures presented as models onto which to predict the TCPs protein structure, we set the closest possible date for the retrieval of PDB models (03 February 2025). The predictions were visualized using ChimeraX v1.9[65]. The best predictions were selected based on pLDDT and PAE values. The figures for the paper were obtained using ChimeraX v1.9.

Author contributions

T.W. designed and performed the experiments, generated and analyzed DAP-Seq and RNA-seq data, conducted phenotypic analyses, and performed EMSA experiments. P.C. contributed to experimental design, RNA-seq data generation, and phenotypic analyses. M.H. generated the isoform mutant and *gt1* mutants used in this study. R.G.H.I., P.H., and R.C.S. contributed to experimental design and scientific discussions. G.W.v.E. conceptualized and supervised the study. T.W. and G.W.v.E. wrote the manuscript with input from all authors.

Acknowledgements

We thank the WUR unifarm personal, for excellent plant care. Simon Kelly for assistance in plant phenotyping during his MSc thesis and Amy Raphaëla for assistance in generating constructs for gene editing during her BSc thesis work.

Funding

This work was financially supported by an Nederlandse organisatie voor Wetenschappelijk Onderzoek (NWO) VIDI grant to G.W.v.E. (project number 18366).

References

1. Huang, X., Hilscher, J., Stoger, E., Christou, P. & Zhu, C. Modification of cereal plant architecture by genome editing to improve yields. *Plant Cell Rep.* **40**, 953–978 (2021).
2. Konishi, S. *et al.* An SNP Caused Loss of Seed Shattering During Rice Domestication. *Science* **312**, 1392–1396 (2006).
3. Pourkheirandish, M. *et al.* Evolution of the Grain Dispersal System in Barley. *Cell* **162**, 527–539 (2015).
4. Simons, K. J. *et al.* Molecular Characterization of the Major Wheat Domestication Gene Q. *Genetics* **172**, 547–555 (2006).
5. Khush, G. S. Green revolution: the way forward. *Nat. Rev. Genet.* **2**, 815–822 (2001).
6. Spielmeyer, W., Ellis, M. H. & Chandler, P. M. Semidwarf (sd-1), "green revolution" rice, contains a defective gibberellin 20-oxidase gene. *Proc. Natl. Acad. Sci.* **99**, 9043–9048 (2002).
7. Liu, L. *et al.* Dissecting the genetic architecture of important traits that enhance wild germplasm resource usage in modern maize breeding. *Mol. Breed.* **39**, 1–11 (2019).
8. van Esse, G. W. The quest for optimal plant architecture. *Science* **376**, 133–134 (2022).
9. Peltonen-Sainio, P., Kangas, A., Salo, Y. & Jauhiainen, L. Grain number dominates grain weight in temperate cereal yield determination: Evidence based on 30 years of multi-location trials. *Field Crops Res.* **100**, 179–188 (2007).
10. Slafer, G. A., Calderini, D. F. & Miralles, D. J. Yield components and compensation in wheat: opportunities for further increasing yield potential. *Increasing Yield Potential Wheat Break. Barriers* 101–133 (1996).
11. Vicentin, L., Canales, J. & Calderini, D. F. The trade-off between grain weight and grain number in wheat is explained by the overlapping of the key phases determining these major yield components. *Front. Plant Sci.* **15**, (2024).

12. Xie, Q. & Sparkes, D. L. Dissecting the trade-off of grain number and size in wheat. *Planta* **254**, 3 (2021).
13. Sukumaran, S., Lopes, M., Dreisigacker, S. & Reynolds, M. Genetic analysis of multi-environmental spring wheat trials identifies genomic regions for locus-specific trade-offs for grain weight and grain number. *Theor. Appl. Genet.* **131**, 985–998 (2018).
14. Liller, C. B., Neuhaus, R., Von Korff, M., Koornneef, M. & Van Esse, W. Mutations in barley row type genes have pleiotropic effects on shoot branching. *PLoS ONE* **10**, (2015).
15. Clark, R. M., Linton, E., Messing, J. & Doebley, J. F. Pattern of diversity in the genomic region near the maize domestication gene tb1. *Proc. Natl. Acad. Sci.* **101**, 700–707 (2004).
16. Igartua, E., Contreras-Moreira, B. & Casas, A. M. TB1: From domestication gene to tool for many trades. *J. Exp. Bot.* **71**, 4621–4624 (2020).
17. Ramsay, L. *et al.* INTERMEDIUM-C, a modifier of lateral spikelet fertility in barley, is an ortholog of the maize domestication gene TEOSINTE BRANCHED 1. *Nat. Genet.* **43**, 169–172 (2011).
18. Takeda, T. *et al.* The OsTB1 gene negatively regulates lateral branching in rice. *Plant J.* **33**, 513–520 (2003).
19. Dixon, L. E., Pasquariello, M. & Boden, S. A. TEOSINTE BRANCHED1 regulates height and stem internode length in bread wheat. *J. Exp. Bot.* **71**, 4742–4750 (2020).
20. Dixon, L. E. *et al.* TEOSINTE BRANCHED1 regulates inflorescence architecture and development in bread wheat (Triticum aestivum). *Plant Cell* **30**, 563–581 (2018).
21. Gaudin, A. C., McClymont, S. A., Soliman, S. S. & Raizada, M. N. The effect of altered dosage of a mutant allele of Teosinte branched 1 (tb1-ref) on the root system of modern maize. *BMC Genet.* **15**, 1–14 (2014).

22. Hubbard, L., McSteen, P., Doebley, J. & Hake, S. Expression patterns and mutant phenotype of teosinte branched1 correlate with growth suppression in maize and teosinte. *Genetics* **162**, 1927–1935 (2002).
23. Martín-Trillo, M. & Cubas, P. TCP genes: a family snapshot ten years later. *Trends Plant Sci.* **15**, 31–39 (2010).
24. de Souza Moraes, T. *et al.* The TCP transcription factor HvTB2 heterodimerizes with VRS5 and controls spike architecture in barley. *Plant Reprod.* 2021.04.14.439785 (2022) doi:10.1007/s00497-022-00441-8.
25. Poursarebani, N. *et al.* COMPOSITUM 1 contributes to the architectural simplification of barley inflorescence via meristem identity signals. *Nat. Commun.* **11**, 1–16 (2020).
26. Coulter, M. *et al.* BaRTv2: a highly resolved barley reference transcriptome for accurate transcript-specific RNA-seq quantification. *Plant J.* **111**, 1183–1202 (2022).
27. Wang, B. *et al.* Unveiling the complexity of the maize transcriptome by single-molecule long-read sequencing. *Nat. Commun.* **7**, 11708 (2016).
28. Jayakodi, M. *et al.* Structural variation in the pangenome of wild and domesticated barley. *Nature* 1–9 (2024) doi:10.1038/s41586-024-08187-1.
29. Zwirek, M., Waugh, R. & McKim, S. M. Interaction between row-type genes in barley controls meristem determinacy and reveals novel routes to improved grain. *New Phytol.* **221**, 1950–1965 (2019).
30. Winkelmolen, T. *et al.* VULGARE ROW-TYPE SIX 5 binds to the promoter of tillering and floral homeotic genes to regulate their expression. *Plant Physiol.* kiaf309 (2025) doi:10.1093/plphys/kiaf309.
31. Shang, Y. *et al.* A CYC/TB1-type TCP transcription factor controls spikelet meristem identity in barley. *J. Exp. Bot.* **71**, 7118–7131 (2020).
32. Dong, Z. *et al.* The regulatory landscape of a core maize domestication module controlling bud dormancy and growth repression. *Nat. Commun.* **10**, 1–15 (2019).

605 33. Whipple, C. J. *et al.* Grassy tillers1 promotes apical dominance in maize and responds
606 to Shade signals in the grasses. *Proc. Natl. Acad. Sci. U. S. A.* **108**, E506–E512 (2011).
607 34. Gonzalez-Grandio, E. *et al.* Abscisic acid signaling is controlled by a BRANCHED1/HD-
608 ZIP i cascade in Arabidopsis axillary buds. *Proc. Natl. Acad. Sci. U. S. A.* **114**, E245–
609 E254 (2017).
610 35. Shanmugaraj, N. *et al.* Multilayered regulation of developmentally programmed pre-
611 anthesis tip degeneration of the barley inflorescence. *Plant Cell*
612 https://doi.org/10.1093/PLCELL/KOAD164 (2023) doi:10.1093/PLCELL/KOAD164.
613 36. Collin, A. *et al.* ABA-induced alternative splicing drives transcriptomic reprogramming
614 for drought tolerance in barley. *BMC Plant Biol.* **25**, 445 (2025).
615 37. Guo, W. *et al.* A barley pan-transcriptome reveals layers of genotype-dependent
616 transcriptional complexity. *Nat. Genet.* **57**, 441–450 (2025).
617 38. Alfonso-Gonzalez, C. & Hilgers, V. (Alternative) transcription start sites as regulators
618 of RNA processing. *Trends Cell Biol.* **34**, 1018–1028 (2024).
619 39. Mejía-Guerra, M. K. *et al.* Core Promoter Plasticity Between Maize Tissues and
620 Genotypes Contrasts with Predominance of Sharp Transcription Initiation Sites. *Plant*
621 *Cell* **27**, 3309–3320 (2015).
622 40. Ozcan, K. E. & Monroe, J. D. Maize β-amylase7 encodes 2 proteins using alternative
623 transcriptional start sites: Nuclear BAM7 and plastidic BAM2. *Plant Physiol.* **192**, 2871–
624 2882 (2023).
625 41. Pavlu, S. *et al.* Core promoterome of barley embryo. *Comput. Struct. Biotechnol. J.* **23**,
626 264–277 (2024).
627 42. Thieffry, A. *et al.* PAMP-triggered genetic reprogramming involves widespread
628 alternative transcription initiation and an immediate transcription factor wave. *Plant*
629 *Cell* **34**, 2615–2637 (2022).

43. Ushijima, T. *et al.* Light Controls Protein Localization through Phytochrome-Mediated Alternative Promoter Selection. *Cell* **171**, 1316-1325.e12 (2017).
44. Sakuma, S. *et al.* Extreme Suppression of Lateral Floret Development by a Single Amino Acid Change in the VRS1 Transcription Factor. *Plant Physiol.* **175**, 1720–1731 (2017).
45. Thirulogachandar, V., Koppolu, R. & Schnurbusch, T. Strategies of grain number determination differentiate barley row types. *J. Exp. Bot.* **72**, 7754–7768 (2021).
46. Komatsuda, T. *et al.* Six-rowed barley originated from a mutation in a homeodomain-leucine zipper I-class homeobox gene. *Proc. Natl. Acad. Sci. U. S. A.* **104**, 1424–1429 (2007).
47. Dang, Y. *et al.* Optimizing sgRNA structure to improve CRISPR-Cas9 knockout efficiency. *Genome Biol.* **16**, 1–10 (2015).
48. Parry, G., Patron, N., Bastow, R. & Matthewman, C. Meeting report: GARNet/OpenPlant CRISPR-Cas workshop. *Plant Methods* **12**, 6 (2016).
49. Hinchliffe, A. & Harwood, W. A. Agrobacterium-mediated transformation of barley immature embryos. *Methods Mol. Biol.* **1900**, 115–126 (2019).
50. Grützner, R. *et al.* High-efficiency genome editing in plants mediated by a Cas9 gene containing multiple introns. *Plant Commun.* **2**, 100135 (2021).
51. Jiang, X. *et al.* FRUITFULL-like genes regulate flowering time and inflorescence architecture in tomato. *Plant Cell* **34**, 1002–1019 (2022).
52. Edgar, R. C. MUSCLE: multiple sequence alignment with high accuracy and high throughput. *Nucleic Acids Res.* **32**, 1792–1797 (2004).
53. Stamatakis, A. RAxML version 8: a tool for phylogenetic analysis and post-analysis of large phylogenies. *Bioinformatics* **30**, 1312–1313 (2014).
54. Hufford, M. B. *et al.* De novo assembly, annotation, and comparative analysis of 26 diverse maize genomes. *Science* **373**, 655–662 (2021).

55. Li, H. Minimap2: pairwise alignment for nucleotide sequences. *Bioinformatics* **34**, 3094–3100 (2018).
56. Thorvaldsdóttir, H., Robinson, J. T. & Mesirov, J. P. Integrative Genomics Viewer (IGV): high-performance genomics data visualization and exploration. *Brief. Bioinform.* **14**, 178–192 (2013).
57. WADDINGTON, S. R., CARTWRIGHT, P. M. & WALL, P. C. A Quantitative Scale of Spike Initial and Pistil Development in Barley and Wheat. *Ann. Bot.* **51**, 119–130 (1983).
58. Bolger, A. M., Lohse, M. & Usadel, B. Trimmomatic: A flexible trimmer for Illumina sequence data. *Bioinformatics* **30**, 2114–2120 (2014).
59. Mascher, M. *et al.* Long-read sequence assembly: a technical evaluation in barley. *Plant Cell* **33**, 1888–1906 (2021).
60. Patro, R., Duggal, G., Love, M. I., Irizarry, R. A. & Kingsford, C. Salmon provides fast and bias-aware quantification of transcript expression. *Nat. Methods* **14**, 417–419 (2017).
61. Love, M. I., Huber, W. & Anders, S. Moderated estimation of fold change and dispersion for RNA-seq data with DESeq2. *Genome Biol.* **15**, 550 (2014).
62. Törönen, P., Medlar, A. & Holm, L. PANNZER2: a rapid functional annotation web server. *Nucleic Acids Res.* **46**, W84–W88 (2018).
63. Abramson, J. *et al.* Accurate structure prediction of biomolecular interactions with AlphaFold 3. *Nature* **630**, 493–500 (2024).
64. Zhang, Y. *et al.* DNA–TCP complex structures reveal a unique recognition mechanism for TCP transcription factor families. *Nucleic Acids Res.* **51**, 434–448 (2023).
65. Meng, E. C. *et al.* UCSF ChimeraX: Tools for structure building and analysis. *Protein Sci.* **32**, e4792 (2023).

Supplementary Files

This is a list of supplementary files associated with this preprint. Click to download.

- Winkelmolenetal2026SupplementaryFigures.pdf
- SupplementaryTables.xlsx